

## Fabrication of Fe<sub>2</sub>CuO<sub>4</sub> nanoparticles via photolysis technique for improved performance in dye-sensitized solar cells

A. F. Kamil<sup>a</sup>, H. I. Abdullah<sup>a</sup>, A. M. Rheima<sup>b,c,d\*</sup>, S. H. Mohammed<sup>c</sup>, S. J. Tuma<sup>a,b</sup>, R. M. Abed<sup>b</sup>

<sup>a</sup>Department of Chemistry, College of Science, Mustansiriyah University, Baghdad, Iraq

<sup>b</sup>Department of Chemistry, College of Science, University of Wasit, kut, Iraq

<sup>c</sup>College of technical engineering, The Islamic University, Najaf, Iraq

<sup>d</sup>Department of pharmacy, Osol Aldeen University College, Baghdad, Iraq

<sup>e</sup>Department of Chemistry, College of education, University of Garmian, kalar, Iraq

This paper created excellent photo-anode materials based on Fe<sub>2</sub>CuO<sub>4</sub> Nanoparticles to efficiently convert the photoelectric into a dye-sensitized solar cell (DSSC). The Fe<sub>2</sub>CuO<sub>4</sub> nanoparticles were prepared via the UV-Irradiation method. The synthesized nanoparticles morphology structure and optical properties were examined using various X-ray diffraction (XRD), Energy Dispersive X-Ray Analysis (EDX) / mapping, field emission scanning electron microscope (FE-SEM), Transmission Electron Microscopy (TEM), and photoluminescence spectroscopy (PL) are examples of these techniques. Transmission electron microscopes (TEM) images validated the Field emission scanning electron microscopy (FE-SEM) and crystal structure of the generated Fe<sub>2</sub>CuO<sub>4</sub> NPs, which had an average particle size of (11.7 nm), and the X-ray diffraction analysis (XRD) investigation indicated no impurity peaks. Photoluminescence spectroscopy (PL) was used to examine the optical characteristics, and the energy gap was found to be 1.95 eV. Nano-powder has been used to develop a successful photo-sensitizing solar cell employing cibacron brilliant red b as a photosensitizer with an efficiency of about 6.47 to 10.39 % energy conversion. We have created a time-saving technology that is simple to regulate, which makes it possible to produce nano-particulate composites without a high testing need. Our findings could investigate an opportunity for nanomaterials to be synthesized with highly rapid answers and now photoanode.

(Received August 14, 2021; Accepted November 16, 2021)

**Keywords:** Dye-sensitized solar cell, Fe<sub>2</sub>CuO<sub>4</sub> nanocomposite, UV-Irradiation method, Cibacron dye

### 1. Introduction

The new heterogeneous subject of nanotechnology has roots in fundamental disciplines; Physics, chemistry, and biology are only a few examples [1, 2]. electrochemistry, photocatalysis, mechanics, energy research, electronics, pharmacy, health care, Chemical sensors, optical devices, food technology, and space exploration are just a few of the fields where nanomaterials are used, as well as textiles of various scales, forms, and chemical compositions and their controlled dispersion. Physical, chemical, and green techniques facilitate nanostructure synthesis [3, 8]. In the last few decades, Bandgap design is already productive with the various transition metals since over half of the visible region corresponds to visible light [9-10]. This is especially true in semiconductors when lowering bandgap energy and increasing visible light absorption. Heterostructures having a single interface that allows for the effective separation and transmission of photogenerated charge carriers can be integrated as heterogeneous catalysts, preventing the recombination of pairs of electron-hole carriers [11,12]. As a result of the synergic ratings of a single metal oxide semiconductor, photoelectrochemical performance can be considerably

---

\* Corresponding author: arahema@uowasit.edu.iq

improved for both semiconductors [13–18]. Hematite ( $\alpha$ - $\text{Fe}_2\text{O}_3$ ) has a small bandgap (1.9–2.2 eV) and is an n-type mineral, non-toxic to the photoanode of the sunshine [19, 20] and has been designated promising for its abundant, cost-effective nature, low-cost, stable, and environmentally compatible [21, 22] synthesis. The  $\alpha$ - $\text{Fe}_2\text{O}_3$  may attain a maximum efficiency of 15% from solar to hydrogen, which is sufficient for practical application. The photocatalyst has a low optical absorption coefficient, poor conductivity, and slow minority carrier diffusion [23, 24]. On either hand, the CuO is a semiconductor p-type of a bandgap in the 1.3–2.21 eV region, with strong absorption and low heat emissions of the solar energy [25, 26]. Both  $\alpha$ - $\text{Fe}_2\text{O}_3$  and CuO have several limits determined by their morphologies, for example, due to the quick recombination of image-generated transport, limited light absorption, load injection, and load separation [25]. Several ways were studied with various semi-conductive materials for increased oxide photo-activity, such as oxygen vacancies technology, doping, catalysts, and heterostructures [27]. By their energy standards, the heterostructures matching the principle have been inserted into several n-type semiconductors with  $\alpha$ - $\text{Fe}_2\text{O}_3$  and show the increased photocatalytic properties under visible light irradiation. [27,28]. Despite some limits, both oxides exhibit a low bandgap and acceptable band edge potentials, making them viable candidates for manufacturing p-n heterostructures[28]. As we know, metal oxides heavily depend on physical, chemical and photochemical properties on their synthesis/construction technology [29, 30]. The aim of this study is to use UV-irradiation to synthesize and analyze a  $\text{Fe}_2\text{CuO}_4$  nanostructure. The nanostructures were employed as photo-anodes in the manufacture of dye-sensitized solar cells when two counter electrodes were used: Graphene oxide-silver nanocomposite (GO-Ag) and (GO)Graphene Oxide Nanosheets.

## 2. Experimental Part

The nanoparticles were made with nickel nitrate  $\text{Cu}(\text{NO}_3)_2$ , iron nitrate  $\text{Fe}(\text{NO}_3)_2$ , sodium hydroxide (NaOH), urea ( $\text{CH}_4\text{N}_2\text{O}$ ) and deionized water. All chemicals were acquired from (BDH) and were not purified in any way.

### 2.1. Synthesis of binary $\text{Fe}_2\text{CuO}_4$ Nanoparticles

Photo- irradiation was employed to generate  $\text{Fe}_2\text{CuO}_4$  nanoparticles. As illustrated in Figure 1, an irradiation cell was used to irradiate  $\text{Cu}(\text{NO}_3)_2$  and  $\text{Fe}(\text{NO}_3)_2$  as  $\text{Fe}_2\text{CuO}_4$  nanoparticle sources. Use a submerged UV source (medium pressure lamp) with a maximum wavelength of 365 nm. The Ultraviolet lamp is submerged in the salt solution, and the quartz tube serves as a cover for it, which is the source of the nanomaterial in the cell. The reactor is a Pyrex tube. An ice bath cools the reactor to avoid rising temperatures due to UV irradiation [31]. Accordingly, 20 ml of 10 mmole  $\text{Cu}(\text{NO}_3)_2$  and 20 ml of 0.01 mole  $\text{Fe}(\text{NO}_3)_2$  were mixed under a magnetic stirrer for 20 min, then 40 ml of 20 mmole urea is progressively added to the solution (drop by drop). The mixture was irradiated by photocell for 30 min with chilling under 5  $^\circ\text{C}$ . Binary superposition is precipitated as a brown-black powder. It is separated and cleaned with deionized water numerous times (all steps done with centrifuge then decantation). The precipitate was dried at 100 $^\circ\text{C}$  for three hours before being calcined at 400 $^\circ\text{C}$  for three hours.  $\text{Fe}_2\text{CuO}_4$  NPs with a red-brown hue have been precipitated.

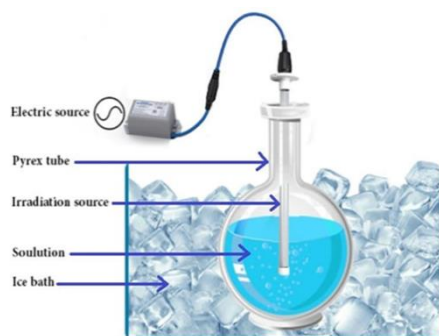


Fig. 1. Image UV-Irradiation cell.

## 2.2. Fabrication of dye-sensitized solar cells

Conductive glass coated with indium tin oxide, which has a resistance of 8 ohm and transmittance of 85%, was washed with solvents (ethanol and deionized water) many times to remove contaminants before being dried with a blower. The following processes were carried out using a DSSC (1.5 \* 2 \* 0.1 cm): To generate a Nano-colloidal of  $\text{Fe}_2\text{CuO}_4$ , nano oxides powder (300 mg) was combined with 10 ml ethyl alcohol. The photo-anodes were made using a dropper to apply a Nano-colloid on the conductive face of the glass for 30 min in the cold before annealing for 30 minutes at 150 °C. After cooling, For sixty minutes, the  $\text{Fe}_2\text{CuO}_4$  nanoparticles electrode (photo-anode) was immersed in cibacron brilliant red B dye (0.5, 1, and 1.5 Molar) [32, 33]. A counter electrode with a conductive glass side covers the Graphene oxide-silver nanocomposite (GO-Ag) and Graphene oxide (GO) nanosheets [34]. The electrolyte solution (I-/I<sup>3-</sup>) was lowered into the working region by capillary action between the photoanode and the counter-electrode. Binder clips were used to keep both electrodes together, as shown in Figure 2.

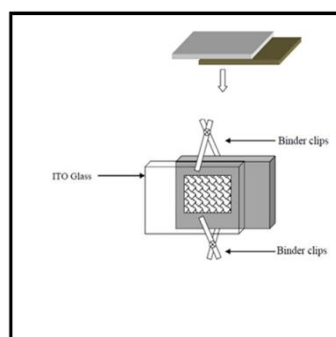


Fig. 2. Image design of dye-sensitized solar cells (DSSCs).

## 3. Results and discussions

Characterization of powders calcination at 400°C has been done using a few approaches. First, the composition of the specimens was investigated using X-ray diffraction (XRD) Model D-5000 with a Cu-K radiation source ( $\lambda=0.154\text{nm}$ ) in  $2\theta$ . Second, the composition and crystalline phase of the as-synthesized pure  $\text{Fe}_2\text{CuO}_4$  composites were investigated by X-ray diffraction (Fig.3), before calcination of  $\text{Fe}(\text{OH})_2\text{-Cu}(\text{OH})_2$ , XRD patterns are observed peaks at 35.96°, 39.44° and 48.78° due to iron and copper hydroxides. As the same figure after calcination at 400°C, XRD pattern is observed peaks at 35.86°, 39.12°, 48.68°, 58.63°, 61.88°, 66.34° and 75.83° due to converted hydroxides to  $\text{Fe}_2\text{CuO}_4$ . The CuO phase is abundant in the XRD pattern obtained from  $\text{Fe}_2\text{CuO}_4$  nanoparticles, coupled with few minor diffractions from the hematite phase, indicating that the composite structure was successfully fabricated. Using the Debye-Scherrer equation, the crystallite size of  $\text{Fe}_2\text{CuO}_4$  was 10.16 nm [31, 34].

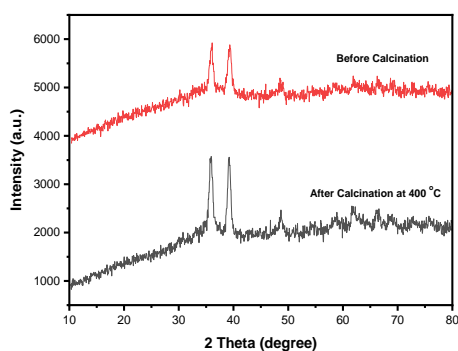


Fig. 3. X-ray diffraction of a prepared sample before and after 400°C calcination.

Model JSM-6010LV of a FE-SEM. The morphology of all produced nanoparticles was investigated using a total of 20 L. Fig. 4 shows the shape of nanoparticles derived by electron microscopy from field emission scanning  $\text{Fe}_2\text{CuO}_4$  (FE-SEM). FE SEM pictures of samples display almost spherical particles with an average size of 15 nm dispersion. Due to the low-temperature impact in synthesis, the FE-SEM pictures are based on a modest degree of aggregation. In the different morphological  $\text{Fe}_2\text{CuO}_4$  nanoparticles, FE-SEM analyses demonstrate the important role of the solution's irradiation-assisted synthesis process.

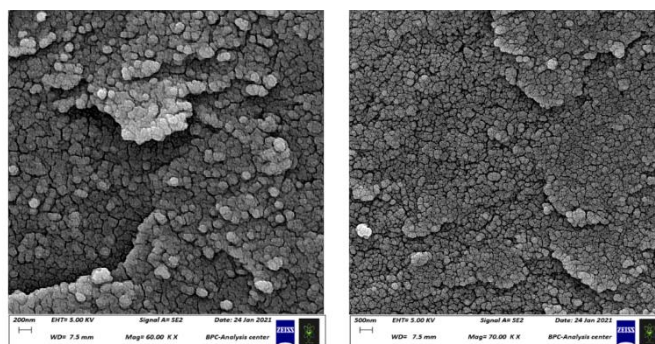


Fig. 4. FE-SEM of sample  $\text{Fe}_2\text{CuO}_4$  Nanoparticles.

The transmission electron microscopic (TEM) micrographs studies also have been performed to assess the optimal particle size, shape and structure information.  $\text{Fe}_2\text{CuO}_4$  nanoparticles formed with the calcination of the samples as prepared and exhibited in Fig. 5. The spherical and consistent morphology of all nanoparticles of the oxides was confirmed in the TEM examinations. The nanoparticles diameters of  $\text{Fe}_2\text{CuO}_4$  are 11.7 nm. Particle sizes of the  $\text{Fe}_2\text{CuO}_4$  nanoparticles derived from TEM research matched closely with the X-ray size derived by X-ray line expansion studies from Scherrer's equation.

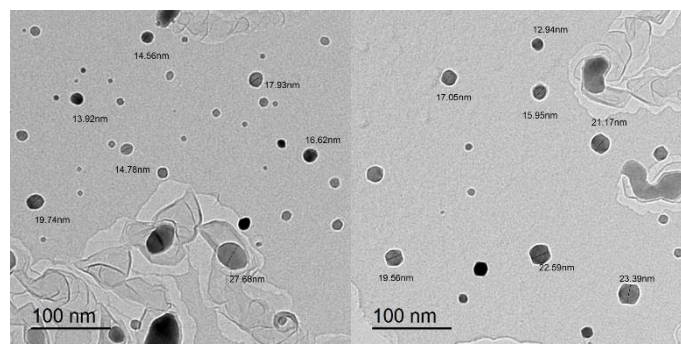


Fig. 5. The TEM of  $Fe_2CuO_4$  nanoparticles.

The EDX spectrum of  $Fe_2CuO_4$  nanoparticles is shown in Fig.6. Typical Iron, Copper, and oxygen peaks are present in the spectrum. The results confirm the high purity of the synthesized nanostructures. Furthermore, the theoretical calculations of the elements agree with the practical estimates obtained from the EDX measurement. Fig.7 indicates that  $Fe_2CuO_4$  NPs have been spread well by the mixed catalyst's matrix. Further data indicate typical images of x-ray mapping to display the distribution of elemental components of a  $\alpha$ - $Fe_2O_3$  and CuO catalyst, which will support the dispersion of the catalyst elements.

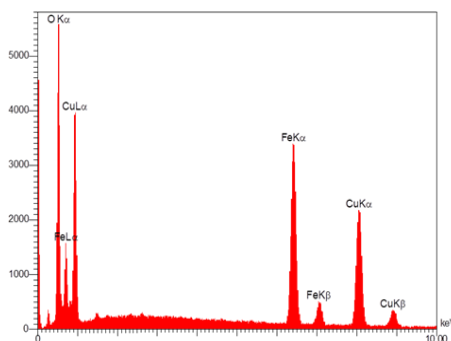


Fig. 6. EDX spectrum of  $Fe_2CuO_4$  NPs.

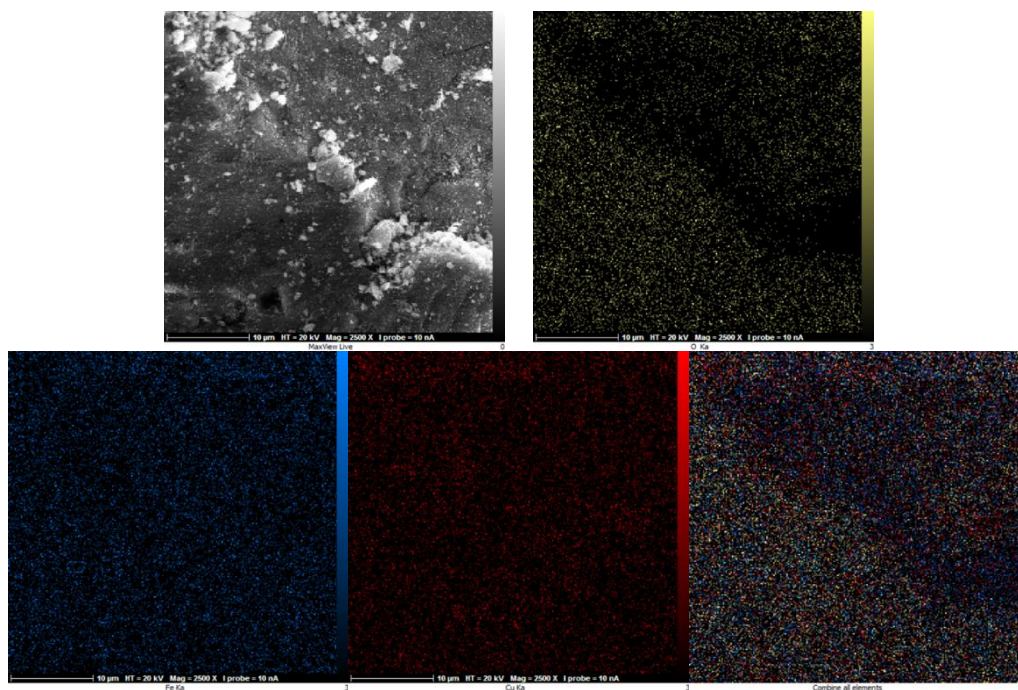


Fig. 7. X-ray mapping of  $Fe_2CuO_4$  NPs.

The  $Fe_2CuO_4$  NPs are homogeneous, with little aggregation. Therefore, the nano-powder of oxides was evaluated for prepared emissions using a solid-state photoluminescent (PL) spectrum. The size distribution of nanoparticles obtained from various sources significantly impacts the PL spectrum's behaviour. Figure 8 shows a single peak with a relatively large whole width at half limit in Photoluminescence Spectroscopy, allowing the emission energy gap to be calculated in this instance. The energy gap was 1.95 eV, by  $E_g (e.V) = 1240/\lambda$  [32].

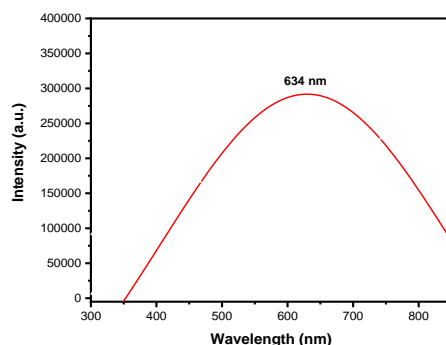


Fig. 8. Photoluminescence Spectroscopy analysis of  $Fe_2CuO_4$  nanoparticles.

### 3.1. Characteristics of dye-sensitized solar cells

The solar cell parameter such as  $I_{sc}$ ,  $V_{oc}$ ,  $J_{max}$ , and  $V_{max}$  FF and cell efficiency were investigated by the current density-voltage (J-V) curve as shown in Fig. 9 and evaluated using equations [32, 33]:

$$\eta = (pm/pin) \times 100\% \quad (1)$$

$$F.F = (J_m * V_m) / (J_{sc} * V_0 c) \quad (2)$$

The characteristics of dye-sensitized solar cells are tabulated in (Table 1). The dyes and small particles sensitizing ratios of  $Fe_2CuO_4$  NPs created were essential for nanoparticles based oxide Solar cell parameters. Graphene (GO) and graphene-Ag (GO-Ag) nanocomposite were employed for counter electrodes. Increased dye Concentration in each cell leads to increased cell power conversion for each counter electrode (GO and GO-Ag). The higher absorption may explain the dye molecules' greater effectiveness on the  $Fe_2CuO_4$  NPs surface. As a result,  $Fe_2CuO_4$  NPs hold promise for future photovoltaics due to the ease with which the procedure may be carried out and the materials produced. The photo-current is the most critical element in determining the total device efficiency limit. Because of their huge surface area and surface energy, parent materials behave differently when particle sizes approach the nanoscale. We found that when dye-sensitized solar cells constructed from GO Nano-sheets were compared to those manufactured from GO-Ag nanocomposite, the electrode generated from GO-Ag nanocomposite had higher efficiency. When silver was connected to graphene oxide, it increased the surface area and conductivity, which improved electron freedom of movement and efficiency [33, 34].

Table 1.  $Fe_2CuO_4$  NPs DSSC characteristics at various concentrations counter electrodes and dye.

counter electrodes	Conc. Dye [M]	$V_{oc}$ (V)	$J_{sc}$ (A/cm <sup>2</sup> )	$V_{max}$ (V)	$J_{max}$ (A/cm <sup>2</sup> )	$P_{max}$ (W/cm <sup>2</sup> )	F.F	$\eta$ %
GO	0.5	0.61	0.0199	0.51	0.0127	0.00647	0.533	6.47
	1	0.65	0.0206	0.53	0.0141	0.00747	0.557	7.47
	1.5	0.66	0.0211	0.54	0.0171	0.00923	0.662	9.23
GO-Ag	0.5	0.63	0.0214	0.52	0.0145	0.00754	0.559	7.54
	1	0.68	0.0229	0.53	0.0182	0.00964	0.619	9.64
	1.5	0.70	0.0237	0.55	0.0189	0.01039	0.626	10.39

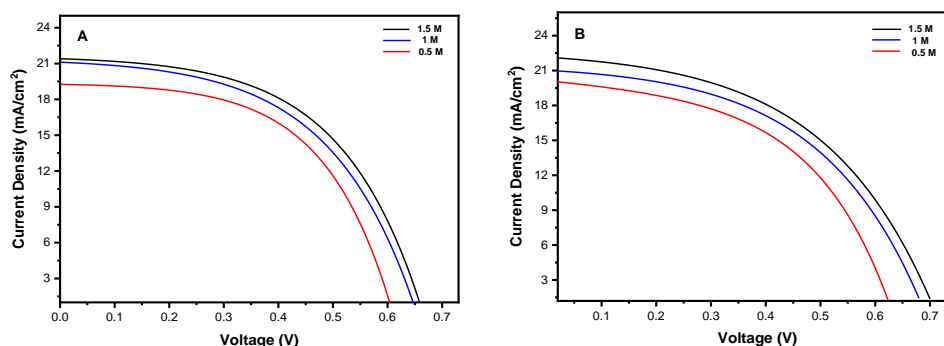


Fig. 9. J -V curves of  $Fe_2CuO_4$  NPs-DSSC at different Concentration dye and counter electrodes A) GO and, B) GO-Ag.

#### 4. Conclusions

Finally, the photolysis approach produced  $Fe_2CuO_4$  NPs successfully. The produced  $Fe_2CuO_4$  NPs have an average crystallite size of 10.16 nm, according to Scherrer's equation. TEM revealed the nanoparticles' spherical nature, with negligible aggregation. The  $Fe_2CuO_4$  NPs have a particle size of 11.7 nm on average. In PL spectroscopy, Broad surface Plasmon resonance absorption peaks with an energy gap of 1.95 eV were seen in  $Fe_2CuO_4$  NPs at max= 634 nanometer. Furthermore,  $Fe_2CuO_4$  NPs electrode containing dye-sensitized solar cells (DSSCs) significantly improves short-circuit current density and open-circuit voltage under simulated sunlight irradiation. The GO-Nano-sheets and GO-Ag nanocomposite used as cathode electrodes, and photosensitizer by dye cibacron brilliant red b. These findings demonstrate that the innovative, low-cost, environmentally-friendly photoanode semiconductor is worth exploring to create higher energy conversion efficiency for future applications.

#### References

- [1] M. A. Mohammed, A. M. Rheima, S. H. Jaber et al., Egyptian Journal of Chemistry **63**(2), 5 (2020).
- [2] A. H. Ismail, H. K. Al-Bairmani, Z. S. Abbas et al., Nano Biomed. Eng. **12**(2), 139 (2020).
- [3] A. A. Ali, R. M. Al-Hassani, D. H. Hussain et al., Drug Invention Today **14**(1), 31 (2020).
- [4] A. F. Kamil, H. I. Abdullah, A. M. Rheima, S. H. Mohammed, Journal of Ovonic Research **17**(3), 2021.
- [5] A. M. Rheima, M. A. Mohammed, S. H. Jaber et al., Drug Invention Today **12**(11), 2818-2819.
- [6] A. M. Rheima, R. S. Mahmood, D. H. Hussain, Z. S. Abbas, Digest Journal of Nanomaterials and Biostructures **15**(4), 2020.
- [7] N. A. Aboud, B. E. Jasim, A. M. Rheima, Chalcogenide Letters **18**(5), 237 (2021).
- [8] A. M. Rheima, M. A. Mohammed, S. H. Jaber et al., Desalination and Water Treatment **194**, 187020.
- [9] H. A. Kadhum, W. M. Salih, A. M. Rheima, Applied Physics A **126**(10), 1 (2020).
- [10] A. M. Rheima, N. A. Aboud, B. E. Jasim, A. H. Ismail, Z. S. Abbas, International journal of pharmaceutical research **13**(1), 342 (2021).
- [11] A. F. Kamil, H. I. Abdullah, A. M. Rheima, S. H. Mohammed, Egyptian Journal of Chemistry, **64** (11) 6137, 2021.
- [12] A. H. Ismail, H. K. AL-Bairmani, Z. S. Abbas et al., Nano Biomed. Eng. **2**(3), 253 (2020).
- [13] A. H. Ismail, H. K. Al-Bairmani, Z. S. Abbas, A. M. Rheima, IOP Conference Series: Materials Science and Engineering **928**(5), 052028 (2020).
- [14] A. H. Ismail, H. K. Al-Bairmani, Egyptian Journal of Chemistry **63**(12), 4951 (2020).
- [15] A. Rheima, A. A. Anber, A. Shakir, A. Salah Hamed, S. Hameed. Iranian Journal of

- Physics Research **20**(3), 51 (2020).
- [16] D. H. Hussain, A. M. Rheima, S. H. Jaber, Egyptian Journal of Chemistry **63**(2), 417 (2020).
- [17] A. M. Rheima, A. A. Anber, H. I. Abdullah, A. H. Ismail, Nano Biomed. Eng. **13**(1), 1 (2021).
- [18] A. F. Kamil, H. I. Abdullah, A. M. Rheima, S. H. Mohammed. Materials Today: Proceedings. 2021 Oct 21.
- [19] A. F. Kamil, H. I. Abdullah, A. M. Rheima, S. H. Mohammed. Materials Today: Proceedings. 2021 Oct 7.
- [20] S.H. Mohammed, A. Rheima, F. Al-jaafari, M. F. Al-Marjani, Z . Abbas. Egyptian Journal of Chemistry. 2021 Oct 24.
- [21] P. Qiu, F. Li, H. Zhang, S. Wang, Z. Jiang, Y. Chen, Electrochimica Acta **358**, 136847 (2020).
- [22] P. Garcia-Muñoz, F. Fresno, A. Víctor, N. Keller, Heterogeneous Photocatalysis, 107 (2020).
- [23] P. K. Kalambate, Z. Rao, J. Wu, Y. Shen, R. Boddula, Y. Huang, Biosensors and Bioelectronics, 112270 (2020).
- [24] A. K. Deb, B. Biswas, N. Goswami, E. F. Hilder, R. Naidu, M. M. Rahman, Applied Surface Science **546**, 149122 (2021).
- [25] Y. Z. Chen, D. J. Jiang, Z. Q. Gong, J. Y. Li, L. N. Wang, International Journal of Minerals, Metallurgy and Materials **27**, 584 (2020).
- [26] R. Parvari, F. Ghorbani-Shahna, A. Bahrami, S. Azizian, M. J. Assari, M. Farhadian, Journal of Photochemistry and Photobiology A: Chemistry **399**, 112643 (2020).
- [27] H. Liu, H. Fu, Y. Liu, X. Chen, K. Yu, L. Wang, Chemosphere **272**, 129534 (2021).
- [28] H. Lu, T. Ju, H. She, L. Wang, Q. Wang, Journal of Materials Science: Materials in Electronics **31**(16), 13787 (2020).
- [29] S. Khelifi, G. Brammertz, L. Choubrac, M. Batuk, S. Yang, M. Meuris, N. Barreau, J. Hadermann, H. Vrielinck, D. Poelman, K. Neyts, Solar Energy Materials and Solar Cells **219**, 110824 (2021).
- [30] H. Filik, A. A. Avan, Arabian Journal of Chemistry, 2020.
- [31] A. M. Rheima, M. A. Mohammed, S. H. Jaber, S. A. Hameed, Journal of Southwest Jiaotong University **54**(5), 2019.
- [32] A. M. Rheima, D. H. Hussain, H. J. Abed, IOP Conference Series: Materials Science and Engineering **928**(5), 052036 (2020)
- [33] N. A. A. Aboud, W. M. Alkayat, D. H. Hussain, A. M. Rheima, A.M., 2020, Journal of Physics: Conference Series **1664**(1), 012094 (2020).
- [34] A. F. Kamil, H. I. Abdullah, A. M. Rheima, WM Khamis, Journal of Ovonic Research **17**(3), 2021.